International Journal of Control, Automation, and Systems VV(X) (YYYY) 1-11
http://dx.doi.org/10.1007/s12555-xxx-xxxx-x
ISSN:1598-6446 eISSN:2005-4092
http://www.springer.com/12555

Geometric Control of a Multirotor UAV with Collective Pitch-Tilting

Jongann Lee , Taekyun Kim , and Dongjun Lee*

Abstract: This paper introduces a controller for the tracking control of a multirotor UAV with collective pitch-tilting, which is capable of generating three-dimensional torque and thrusts in both the upward and forward directions of the vehicle. This vehicle design offers several advantages over traditional multirotors, including the ability to exert a frontal force without changing attitude, which is beneficial for aerial manipulation, and the capability to orient the front of the vehicle in any direction, making it ideal for surveillance applications. We show that the system dynamics of the multirotor with collective pitch-tilting is differentially flat with its center of mass position, yaw angle, and pitch angle being the flat outputs. To track trajectories of the flat outputs, we propose a geometric tracking controller based on the nonlinear SE(3) dynamics of the vehicle, which makes the controller free of linearization errors and singularities. The controller exhibits desirable closed-loop properties, with the ability to recover from a near-inverted attitude, which is proven using Lyapunov analysis. A numerical simulation of the controller showcases the stability and efficacy of the proposed controller.

Keywords: Differential Flatness, Geometric Tracking Controller, Lyapunov Analysis, Multirotor with Collective Pitch-Tilting

1. INTRODUCTION

Multirotors have emerged as the dominant UAV form factor due to their superior accessibility, maneuverability, capacity for onboard sensors, and applicability to a wide range of applications [1]. Conventional multirotors are typically designed with multiple rotors arranged in the same plane and oriented vertically. This design enables the utilization of fixed-pitch propellers, with control input solely determined by the rotation speed of the propeller. As a result, these platforms are mechanically simple and exhibit well-understood control properties. Notwithstanding their simplicity, they are very maneuverable and can hover stably in adverse conditions [2].

However, multirotors have an inherent limitation: they are underactuated platforms, meaning the number of control inputs is less than the degrees of freedom. All the rotors on a multirotor generate thrust in the same direction and are therefore incapable of generating lateral thrust. Consequently, simultaneous control of both the position and orientation of the vehicle is impossible. For example, under calm conditions, multirotors cannot hover unless their pitch and roll are set to zero degrees.

As a consequence, multirotors are unsuitable for certain applications. Aerial manipulation has emerged as a prominent research focus for UAVs; however, the underactuation of the multirotor platform severely constrains its efficacy in this domain. Even minor disturbances, such as sideways gusts, necessitate adjustments in the platform's orientation, making it difficult to maintain contact or to continue the manipulation effort. Moreover, tasks such as the examination of tunnel walls, ceilings, and complex structures pose further challenges to multirotors, as their inherent limitation impedes the camera from maintaining the desired orientation without additional actuation.

Hence, addressing the underactuation problem is crucial for enhancing the versatility of UAVs across diverse applications. The solution to this challenge is relatively straightforward: augment the vehicle with additional control degrees of freedom, enabling it to track arbitrary SE(3) trajectories. Indeed, numerous fully actuated UAV designs have previously been proposed [3]. These designs employ at least 6 rotors and/or actuated joints, enabling the generation of lateral thrust without necessitating alterations in its attitude [4], [5], [6], [7].

Nevertheless, increasing the number of actuators introduces certain drawbacks, including heightened mechanical complexity, reduced power efficiency, and increased complexity in control system design. Thus, it is preferable to minimize the number of actuators given the require-

Manuscript received Month XX, 2024; revised Month XX, 2024; accepted Month XX, 2024. Recommended by Associate Editor OOO under the direction of Editor OOO. This journal was supported by the National Research Foundation of Korea (NRF) grant funded by the Korea government (MSIT) (No. NRF2020R1A2C3010039).

Jongann Lee is with the Department of Aeriospace Enginnering, Seoul National University, Seoul 08826, Korea (e-mail: johnny3357@snu.ac.kr). Taekyun Kim and Dongjun Lee are with the Department of Mechanical Engineering, IAMD and IOER, Seoul National University, Seoul 08826, Korea (emails: {ktk4532, djlee} @snu.ac.kr).
* Corresponding author.

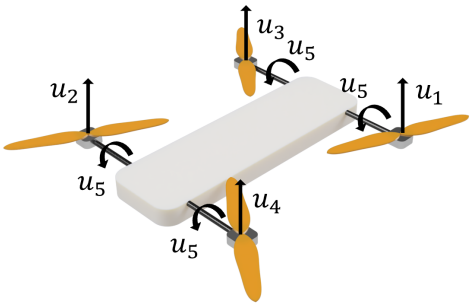

Fig. 1. 3D diagram of a multirotor UAV with collective pitch-tilting

ments. This paper aims to address these considerations by focusing on multirotors with collective pitch-tilting, which can generate thrust in both the vertical and frontal axes.

A diagram of the multirotor with collective pitch-tilting is depicted in Fig. 1. The vehicle is configured such that the rotors of the quadrotor can tilt collectively in a single direction, thereby introducing an additional control degree of freedom. The multirotor with collective pitch-tilting is a more capable aerial manipulation platform as it allows the vehicle to exert a frontal force without changing its attitude. Additionally, this configuration is also beneficial for surveillance applications as full control of the pitch and yaw angles enables the camera to be directed toward any desired direction.

Previous research has explored the development of such vehicles, employing either a closed loop PID controller or an open source controller like PX4 [8], [9], [10]. Indeed, the vehicles discussed so far predominantly rely on closed-loop PID controllers for their control systems. Despite their effectiveness in stabilizing near-zero attitude error, PID controllers exhibit limitations in regions of significant attitude error due to their reliance on the small angle approximation. Furthermore, it's noteworthy that none of the mentioned controllers possess trajectory tracking capabilities; their functionalities typically extend to maintaining a reference attitude or sustaining a fixed position. While a trajectory tracking controller for the multirotor with collective pitch-tilting that circumvents the small angle approximation has been proposed [11], the usage of inverted matrices renders it vulnerable to singularities at certain orientations.

In [12], the authors proposed a geometric tracking controller for quadrotor type UAVs, which addresses the previously mentioned shortcomings by leveraging the $\mathrm{SO}(3)$ manifold for attitude control [12]. While this controller has been adapted for use with fully actuated multirotors [13], it has yet to be tailored for the multirotor with collective pitch-tilting.

In this paper, we propose a trajectory tracking controller for the multirotor with collective pitch-tilting, which builds on the geometric controller for quadrotor-type UAVs in [12], and addresses the previously mentioned shortcomings by leveraging the $\mathrm{SO}(3)$ manifold for attitude control. To derive the proposed geometric controller, we first define the coordinate system and dynamics model for the multirotor with collective pitch-tilting. Following the property that a smooth trajectory expressed by a differentially flat output can be tracked by the system, we then derive the differentially flat output for the multirotor with collective pitch-tilting. Finally, we design a controller to track the trajectory represented by the flat output and prove its convergence through Lyapunov analysis. The effectiveness of the proposed controller is validated in numerical simulations, demonstrating its ability to track the trajectory even in cases of significant attitude error where other controllers would fail.

The paper is structured as follows: Section 2 establishes the vehicle model and specifies its dynamics. In Section 3, a set of state variables, encompassing position, yaw, and pitch, is shown to be a differentially flat output of the dynamics of the multirotor with collective pitch-tilting. We then design a geometric controller tailored for the vehicle under consideration in Section 4 and provide a proof of its exponential stability. To illustrate its performance, a numerical simulation is presented in Section 5, followed by some concluding remarks in Section 6.

2. MODEL AND DYNAMICS

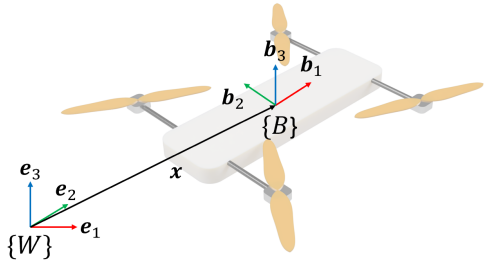

Fig. 2. Model of the multirotor with collective pitch-tilting

The model of the multirotor with collective pitch-tilting employs two coordinate frames: the world frame W and the body frame B, shown in Fig. 2. The body frame B adopts a "North-West-Up" coordinate system, with the origin set as the center of mass of the vehicle. The x-axis of the body frame $\mathbf{b}_1$ is the forward direction, the y-axis $\mathbf{b}_2$ points to the left, and the z-axis $\mathbf{b}_3$ points upwards. The reference world frame W also has its z-axis $\mathbf{e}_3$ pointing upwards, in the direction opposite to gravity.

The position of the center of mass is denoted as $\mathbf{x} = [x\ y\ z]^T \in \mathbb{R}^3$ and its velocity is denoted as $\mathbf{v} \in \mathbb{R}^3$. The

rotation matrix of the vehicle with respect to the world frame is written as $\mathbf{R}_{WB} \in \mathrm{SO}(3)$, where $\mathbf{R}_{WB} = [\mathbf{b}_1\ \mathbf{b}_2\ \mathbf{b}_3]$. For trajectory generation, Z-Y-X Euler angles are utilized, with the z-rotation being yaw(ψ), y-rotation being pitch(θ), and x-rotation being roll(ϕ). $\boldsymbol{\omega}_{BB}$ stands for the angular velocity of the vehicle with respect to the body frame.

The vehicle is modeled as a rigid body with constant mass m and moment of inertia $\mathbf{J}$. Its orientation is fully actuated and it can generate thrust independently in two directions. The torque control input in the body frame B is denoted as $\boldsymbol{\tau} \in \mathbb{R}^3$. The thrust in the $\mathbf{b}_1$ direction is denoted as $f_x \in \mathbb{R}$, while the thrust in the $\mathbf{b}_3$ direction is denoted as $f_z \in \mathbb{R}$.

With the above definitions, the dynamics of the vehicle is expressed as follows [14]:

$$\dot{\mathbf{x}} = \mathbf{v}, \tag{1}$$

$$m\dot{\mathbf{v}} = -mg\mathbf{e}_3 + f_x\mathbf{b}_1 + f_z\mathbf{b}_3, \tag{2}$$

$$\dot{\mathbf{R}}_{WB} = \mathbf{R}_{WB}\hat{\boldsymbol{\omega}}_{BB}, \tag{3}$$

$$\mathbf{J}\dot{\boldsymbol{\omega}}_{BB} = \boldsymbol{\tau} - \hat{\boldsymbol{\omega}}_{BB}\mathbf{J}\boldsymbol{\omega}_{BB}, \tag{4}$$

where the hat map $\hat{(\cdot)} : \mathbb{R}^3 \to \mathrm{so}(3)$ is defined such that $\hat{\mathbf{x}}\mathbf{y} = \mathbf{x} \times \mathbf{y}$ for all $\mathbf{x}, \mathbf{y} \in \mathbb{R}^3$.

3. DIFFERENTIAL FLATNESS

It is well known that the quadrotor dynamics with regards to four inputs is differentially flat [15]. This means that the state of the quadrotor and its four inputs can be written as an algebraic function of the four flat outputs and their derivatives.

In this section, we show that the following set of state variables $\boldsymbol{\sigma}$ is the flat output of the dynamics of the multirotor with collective pitch-tilting.

$$\boldsymbol{\sigma} = [x\ y\ z\ \psi\ \theta]^T \tag{5}$$

Furthermore, we present the explicit derivation of the state variables and inputs in (1)-(4) represented by the flat outputs, which is required for the proposed controller in Section 4.

The position, velocity, and acceleration of the center of mass are directly obtained by the first three terms in $\boldsymbol{\sigma}$ and its derivatives. To express the rotation matrix $\mathbf{R}_{WB}$ as a function of $\boldsymbol{\sigma}$ and its derivatives, the individual body frame unit vectors $\mathbf{b}_1$, $\mathbf{b}_2$, and $\mathbf{b}_3$ are derived. First, $\mathbf{b}_1$ is determined using the yaw and pitch angles.

$$\mathbf{b}_1 = \mathrm{Rot}_z(\psi)\mathrm{Rot}_y(\theta)[1\ 0\ 0]^T \tag{6}$$

To determine the other two unit vectors, we define a force vector $\mathbf{f}_t = m[\ddot{x}\ \ddot{y}\ \ddot{z}+g]^T$ required to move the vehicle along the trajectory. As this vehicle is capable of creating thrust along the x and z axes, the force vector can be expressed by $\mathbf{f}_t = f_x\mathbf{b}_1 + f_z\mathbf{b}_3$. From (6), we can derive the x and z direction thrust values as

$$\begin{aligned} f_x &= \mathbf{f}_t \cdot \mathbf{b}_1, \\ f_z &= \|\mathbf{f}_t - f_x\mathbf{b}_1\|. \end{aligned} \tag{7}$$

Then, $\mathbf{R}_{WB}$ can be defined with the remaining unit vectors as

$$\begin{aligned} \mathbf{b}_3 &= \frac{\mathbf{f}_t - f_x\mathbf{b}_1}{f_z}, \\ \mathbf{b}_2 &= \mathbf{b}_3 \times \mathbf{b}_1. \end{aligned} \tag{8}$$

To derive the angular velocity and angular acceleration, we define an intermediate reference frame C, which is rotated by the yaw and pitch angle with respect to the world frame as

$$\mathbf{R}_{WC} = \mathrm{Rot}_z(\psi)\mathrm{Rot}_y(\theta). \tag{9}$$

Then, the rotation from frame C to frame B only involves an x-axis rotation as $\mathbf{R}_{CB} = \mathrm{Rot}_x(\phi)$.

Here, we represent the angular velocity of the vehicle in the world frame as $\boldsymbol{\omega}_{BW} = p\mathbf{b}_1 + q\mathbf{b}_2 + r\mathbf{b}_3$. From the derivative of (2), we get

$$m\mathbf{x}^{(3)} = \dot{f}_x\mathbf{b}_1 + f_x(\boldsymbol{\omega}_{BW} \times \mathbf{b}_1) + \dot{f}_z\mathbf{b}_3 + f_z(\boldsymbol{\omega}_{BW} \times \mathbf{b}_3). \tag{10}$$

Using the body frame component notation for $\boldsymbol{\omega}_{BW}$, (10) yields the following equations.

$$\dot{f}_x = m\mathbf{x}^{(3)} \cdot \mathbf{b}_1 - f_z q, \tag{11}$$

$$\dot{f}_z = m\mathbf{x}^{(3)} \cdot \mathbf{b}_3 + f_x q, \tag{12}$$

$$p = \frac{f_x r - m\mathbf{x}^{(3)} \cdot \mathbf{b}_2}{f_z}. \tag{13}$$

Since, the rotation from frame C to frame B only involves an x-axis rotation, the angular velocity of frame B with respect to frame C, $\boldsymbol{\omega}_{BC}$, has no $\mathbf{b}_2$ and $\mathbf{b}_3$ components. From the relation of $\boldsymbol{\omega}_{BW} = \boldsymbol{\omega}_{CW} + R_{WC}\boldsymbol{\omega}_{BC}$, we find that the $\mathbf{b}_2, \mathbf{b}_3$ components of $\boldsymbol{\omega}_{BW}$ are identical to those of $\boldsymbol{\omega}_{CW}$. Since $\boldsymbol{\omega}_{CW}$ can be determined from the yaw/pitch and their derivatives, q and r can also be determined as

$$q = \boldsymbol{\omega}_{CW} \cdot \mathbf{b}_2,\ r = \boldsymbol{\omega}_{CW} \cdot \mathbf{b}_3, \tag{14}$$

where

$$\boldsymbol{\omega}_{CW} = \begin{bmatrix} -\dot{\theta}\sin(\psi) \\ \dot{\theta}\cos(\psi) \\ \dot{\psi} \end{bmatrix}. \tag{15}$$

Using the r in (14), we can obtain p from (13), thus completing the derivation of $\boldsymbol{\omega}_{BW}$. Then, we can get the body angular velocity from $\boldsymbol{\omega}_{BB} = \mathbf{R}_{WB}^T\boldsymbol{\omega}_{BW}$.

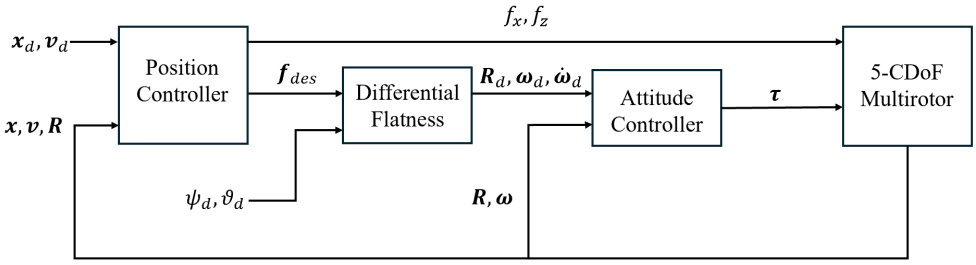

Fig. 3. Diagram of the proposed controller

The angular acceleration can be obtained in a similar manner. First, the derivative of (10) is

$$\begin{aligned} m\mathbf{x}^{(4)} = {} & \ddot{f}_x\mathbf{b}_1 + 2\dot{f}_x(\boldsymbol{\omega}_{BW}\times\mathbf{b}_1) + \ddot{f}_z\mathbf{b}_3 + 2\dot{f}_z(\boldsymbol{\omega}_{BW}\times\mathbf{b}_3) \\ & + f_x(\boldsymbol{\omega}_{BW}\times(\boldsymbol{\omega}_{BW}\times\mathbf{b}_1)) + f_x(\dot{\boldsymbol{\omega}}_{BW}\times\mathbf{b}_1) \\ & + f_z(\boldsymbol{\omega}_{BW}\times(\boldsymbol{\omega}_{BW}\times\mathbf{b}_3)) + f_z(\dot{\boldsymbol{\omega}}_{BW}\times\mathbf{b}_3). \end{aligned} \tag{16}$$

Denoting $\dot{\omega}_{BW} = p'\mathbf{b}_1 + q'\mathbf{b}_2 + r'\mathbf{b}_3$, we can derive a relation for p' as follows:

$$p' = \frac{-m\mathbf{x}^{(4)}\cdot\mathbf{b}_2 + 2\dot{f}_x r - 2\dot{f}_z p + f_x pq + f_z qr + f_x r'}{f_z}, \tag{17}$$

where $\dot{f}_x$ and $\dot{f}_z$ are the values from (11) and (12).

Regarding q', r', they can also be entirely determined from the yaw/pitch and their derivatives. From the relation $\boldsymbol{\omega}_{BW} = \boldsymbol{\omega}_{CW} + R_{WC}\boldsymbol{\omega}_{BC}$, its derivative yields $\dot{\boldsymbol{\omega}}_{BW} = \dot{\boldsymbol{\omega}}_{CW} + R_{WC}\dot{\boldsymbol{\omega}}_{BC} + \boldsymbol{\omega}_{CW}\times\boldsymbol{\omega}_{BW}$. The calculation is simplified by the fact that $\dot{\boldsymbol{\omega}}_{BC}$ has no $\mathbf{b}_2, \mathbf{b}_3$ component as follows:

$$\begin{aligned} q' &= (\dot{\boldsymbol{\omega}}_{CW} + \boldsymbol{\omega}_{CW}\times\boldsymbol{\omega}_{BW})\cdot\mathbf{b}_2, \\ r' &= (\dot{\boldsymbol{\omega}}_{CW} + \boldsymbol{\omega}_{CW}\times\boldsymbol{\omega}_{BW})\cdot\mathbf{b}_3, \end{aligned} \tag{18}$$

where $\boldsymbol{\omega}_{CW}, \boldsymbol{\omega}_{BW}$ are the values calculated earlier and $\dot{\boldsymbol{\omega}}_{CW}$ is given by

$$\dot{\boldsymbol{\omega}}_{CW} = \begin{bmatrix} -\ddot{\theta}\sin(\psi) - \dot{\psi}\dot{\theta}\cos(\psi) \\ \ddot{\theta}\cos(\psi) - \dot{\psi}\dot{\theta}\sin(\psi) \\ \ddot{\psi} \end{bmatrix}. \tag{19}$$

Lastly, we can get the body angular acceleration from $\dot{\boldsymbol{\omega}}_{BB} = \mathbf{R}_{WB}^T\dot{\boldsymbol{\omega}}_{BW}$ and then the body torque $\boldsymbol{\tau}$ from (4).

4. CONTROLLER DESIGN

In this section, we present the controller for the multirotor with collective pitch-tilting, which is a modified version of the geometric tracking controller by Taeyoung Lee [12]. This controller utilizes error feedback in position, velocity, attitude, and angular velocity. Terms that compensate for the dynamics of the vehicle are incorporated. The overall controller structure is illustrated in Fig. 3.

4.1. Trajectory Errors

The desired trajectory is comprised of the coordinates of the center of mass $\mathbf{x}_d = [x_d\ y_d\ z_d]^T \in \mathbb{R}^3$, the yaw angle $\psi_d \in \mathbb{S}^1$, and the pitch angle $\theta_d \in (-\frac{\pi}{2}, \frac{\pi}{2})$. The following assumption is made about the desired acceleration for a given positive constant B.

$$\|mg\mathbf{e}_3 + m\ddot{\mathbf{x}}_d\| < B \tag{20}$$

The results of the previous section on differential flatness allow us to define the desired attitude $\mathbf{R}_d$, desired angular velocity $\boldsymbol{\omega}_d$, and the desired angular acceleration $\dot{\boldsymbol{\omega}}_d$ with respect to the body frame. However, it's important to note that the values obtained in the previous section assume the vehicle is already on the desired trajectory. In the real-time controller, the vehicle is likely not on the desired trajectory, and so $\mathbf{R}_d, \boldsymbol{\omega}_d, \dot{\boldsymbol{\omega}}_d$ is defined differently. For brevity, we will drop the frame subscripts for the attitude and angular velocity as $\mathbf{R} = \mathbf{R}_{WB}$, and $\boldsymbol{\omega} = \boldsymbol{\omega}_{BB}$.

Following [12], we define the trajectory tracking error terms as follows: 1) the position and velocity tracking errors are $\mathbf{e}_x := \mathbf{x} - \mathbf{x}_d$, $\mathbf{e}_v := \mathbf{v} - \mathbf{v}_d$; 2) the real-valued error function on SO(3) is $\Psi(\mathbf{R}, \mathbf{R}_d) := \frac{1}{2}\mathrm{tr}(\mathbf{I} - \mathbf{R}_d^T\mathbf{R})$, which is locally positive-definite about $\mathbf{R} = \mathbf{R}_d$ within the region where the rotation angle between $\mathbf{R}$ and $\mathbf{R}_d$ is less than 180° [16]; 3) the attitude tracking error is $\mathbf{e}_R := \frac{1}{2}\left(\mathbf{R}_d^T\mathbf{R} - \mathbf{R}^T\mathbf{R}_d\right)^\vee$, where the vee map $\vee : so(3) \to \mathbb{R}^3$ is defined as the inverse of the hat map; and 4) the angular velocity tracking error is $\mathbf{e}_\omega = \boldsymbol{\omega} - \mathbf{R}^T\mathbf{R}_d\boldsymbol{\omega}_d$.

4.2. Control Law

Using the defined errors and positive constants k_x and k_v, we can calculate the desired force vector $\mathbf{f}_{des}$ which makes the position and velocity errors converge to zero.

$$\mathbf{f}_{des} = -k_x\mathbf{e}_x - k_v\mathbf{e}_v + mg\mathbf{e}_3 + m\ddot{\mathbf{x}}_d \tag{21}$$

However, the multirotor with collective pitch-tilting can only generate thrust in the $\mathbf{b}_1$ and $\mathbf{b}_3$ direction. Therefore, we adopt the thrust control input f_x, f_z as the projection of $\mathbf{F}_{des}$ on the $\mathbf{b}_1, \mathbf{b}_3$ axis respectively.

$$f_x = \mathbf{f}_{des}\cdot\mathbf{b}_1,\ f_z = \mathbf{f}_{des}\cdot\mathbf{b}_3 \tag{22}$$

We now calculate the desired attitude $\mathbf{R}_d$. $\mathbf{b}_{1d}$ is defined using the desired yaw and pitch, while $\mathbf{b}_{2d}$ and $\mathbf{b}_{3d}$ are defined using the desired force $\mathbf{f}_{des}$.

$$\begin{aligned}\mathbf{b}_{1d} &= \mathrm{Rot}_z(\psi_d)\mathrm{Rot}_y(\theta_d)[1\ 0\ 0]^T,\\ \mathbf{b}_{3d} &= \frac{\mathbf{f}_{des}-(\mathbf{f}_{des}\cdot\mathbf{b}_{1d})\mathbf{b}_{1d}}{\|\mathbf{f}_{des}-(\mathbf{f}_{des}\cdot\mathbf{b}_{1d})\mathbf{b}_{1d}\|},\\ \mathbf{b}_{2d} &= \mathbf{b}_{3d}\times\mathbf{b}_{1d}.\end{aligned} \tag{23}$$

Here $\mathbf{f}_{des}-(\mathbf{f}_{des}\cdot\mathbf{b}_{1d})\mathbf{b}_{1d}\neq 0$ is assumed in order to properly define $\mathbf{b}_{3d}$.

The desired angular velocity $\boldsymbol{\omega}_d$ and desired angular acceleration $\dot{\boldsymbol{\omega}}_d$ are determined using the method described in the previous section.

With all the necessary variables determined, the torque control input is defined as follows, given positive constants k_R and k_ω.

$$\begin{aligned}\boldsymbol{\tau} = &-k_R\mathbf{e}_R - k_\omega\mathbf{e}_\omega + \boldsymbol{\omega}\times\mathbf{J}\boldsymbol{\omega}\\ &-\mathbf{J}(\hat{\boldsymbol{\omega}}\mathbf{R}^T\mathbf{R}_d\boldsymbol{\omega}_d - \mathbf{R}^T\mathbf{R}_d\dot{\boldsymbol{\omega}}_d)\end{aligned} \tag{24}$$

The torque input is the same as that of the quadrotor geometric tracking controller [12].

In summary, this controller is designed to ensure the vehicle's position error converges to zero when there is no attitude error. The torque input is employed to rapidly correct any attitude error, thereby achieving asymptotic stability of the complete dynamics.

4.3. Controlled System Stability

The stability of the proposed controller is demonstrated in three stages. First, we prove the exponential stability of the attitude dynamics when the initial attitude error is less than 180°. Second, we show that the complete dynamics is exponentially stable when the initial attitude error is less than 90°. Lastly, we establish the exponential attractiveness of the position error for initial attitude errors between 90° and 180°.

The following proposition states that the attitude dynamics of the vehicle is exponentially stable for an initial attitude error of less than 180°.

Proposition 1: Consider the torque input $\boldsymbol{\tau}$ defined by (24), with positive constants k_R, k_Ω. Suppose that the initial conditions satisfy

$$\begin{aligned}&\Psi(\mathbf{R}(0),\mathbf{R}_d(0)) < 2,\\ &\|\mathbf{e}_\omega(0)\|^2 < \frac{2}{\lambda_{\max}(\mathbf{J})}k_R(2-\Psi(\mathbf{R}(0),\mathbf{R}_d(0))).\end{aligned} \tag{25}$$

Then the zero equilibrium of the attitude tracking error $\mathbf{e}_R, \mathbf{e}_\omega$ is exponentially stable. Furthermore, there exist constants $\alpha_2, \beta_2 > 0$ such that

$$\Psi(\mathbf{R}(t),\mathbf{R}_d(t)) \le \min\{2, \alpha_2 e^{-\beta_2 t}\}. \tag{26}$$

Proof: See Appendix A.1.

We now discuss the stability of the position dynamics. For an underactuated platform like the multirotor with collective pitch-tilting, applying a desired force input requires the vehicle to be in a certain desired orientation. Thus, the position dynamics can be stable only if the attitude dynamics are stable. With the stability of the attitude dynamics established in Proposition 1, we present and prove Proposition 2, which establishes that the tracking errors of the complete system exponentially converge to zero given an initial attitude error of less than 90°.

Proposition 2: Consider the force inputs f_x, f_z and the torque input $\boldsymbol{\tau}$ as defined in (22) and (24). Suppose that the initial conditions satisfy

$$\Psi(\mathbf{R}(0),\mathbf{R}_d(0)) \le \psi_1 < 1, \tag{27}$$

$$\|\mathbf{e}_x(0)\| < e_{x_{\max}}, \tag{28}$$

where $\psi_1, e_{x_{\max}}$ are the maximum allowed attitude and position error. Define $\mathbf{W}_1, \mathbf{W}_{12}, \mathbf{W}_2 \in \mathbb{R}^{2\times 2}$ to be

$$\begin{aligned}\mathbf{W}_1 &= \begin{bmatrix}\frac{c_1k_x}{m}(1-\alpha) & -\frac{c_1k_v}{2m}(1+\alpha)\\ -\frac{c_1k_v}{2m}(1+\alpha) & k_v(1-\alpha)-c_1\end{bmatrix},\\ \mathbf{W}_{12} &= \begin{bmatrix}\frac{c_1}{m}B & 0\\ B+k_xe_{x_{\max}} & 0\end{bmatrix},\\ \mathbf{W}_2 &= \begin{bmatrix}\frac{c_2k_R}{\lambda_{\max}(\mathbf{J})} & -\frac{c_2k_\omega}{2\lambda_{\min}(\mathbf{J})}\\ -\frac{c_2k_\omega}{2\lambda_{\min}(\mathbf{J})} & k_\omega - c_2\end{bmatrix},\end{aligned} \tag{29}$$

where B is from (20), $\alpha = \sqrt{\psi_1(2-\psi_1)}$, and $c_1, c_2 \in \mathbb{R}$. For any positive constants k_x, k_v, we choose the positive constants c_1, c_2, k_R, k_ω such that

$$\begin{aligned}c_1 < \min\Bigg\{&k_v(1-\alpha),\\ &\frac{4mk_xk_v(1-\alpha)}{k_v^2(1+\alpha)^2+4mk_x(1-\alpha)}, \sqrt{k_xm}\Bigg\},\end{aligned} \tag{30}$$

$$\begin{aligned}c_2 < \min\Bigg\{&k_\omega, \frac{4k_\omega k_R\lambda_{\min}(\mathbf{J})^2}{k_\omega^2\lambda_{\max}(\mathbf{J})+4k_R\lambda_{\max}(\mathbf{J})^2},\\ &\sqrt{k_R\lambda_{\min}(\mathbf{J})}\Bigg\},\end{aligned} \tag{31}$$

$$\lambda_{\min}(\mathbf{W}_2) > \frac{4\|\mathbf{W}_{12}\|^2}{\lambda_{\min}(\mathbf{W}_1)}. \tag{32}$$

Then the zero equilibrium of the tracking errors of the complete system is exponentially stable. The region of attraction is defined by (27),(28), and the following equations.

$$\|\mathbf{e}_\omega(0)\|^2 < \frac{2}{\lambda_{\max}(\mathbf{J})}k_R(1-\Psi(\mathbf{R}(0),\mathbf{R}_d(0))), \tag{33}$$

$$\lambda_{\max}(\mathbf{M}_{12})\|\mathbf{z}_1(0)\|^2 + \lambda_{\max}(\mathbf{M}_{22})\|\mathbf{z}_2(0)\|^2 < \frac{1}{2}k_xe_{x_{\max}}^2 \tag{34}$$

Here $\mathbf{z}_1 = [\|\mathbf{e}_x\|,\ \|\mathbf{e}_v\|]^T$, $\mathbf{z}_2 = [\|\mathbf{e}_R\|,\ \|\mathbf{e}_\omega\|]^T$, and the matrices $\mathbf{M}_{12}, \mathbf{M}_{22}$ are defined as

$$\mathbf{M}_{12} = \frac{1}{2}\begin{bmatrix} k_x & c_1 \\ c_1 & m \end{bmatrix}, \mathbf{M}_{22} = \frac{1}{2}\begin{bmatrix} \frac{2k_R}{2-\psi_1} & c_2 \\ c_2 & \lambda_{\max}(\mathbf{J}) \end{bmatrix}. \tag{35}$$

Proof: See Appendix A.2.

The exponential stability of the complete dynamics has been demonstrated for an attitude error of less than 90°, i.e., $\Psi(\mathbf{R}(0), \mathbf{R}_d(0)) < 1$. For an initial condition where $1 \leq \Psi(\mathbf{R}(0), \mathbf{R}_d(0)) < 2$, proposition 1 remains valid, and the attitude dynamics exhibit exponential stability. Consequently, the attitude error function Ψ exponentially decreases to a value less than 1 in a finite amount of time. Therefore, the complete dynamics is almost globally exponentially attractive [17].

Proposition 3: Suppose that the same design conditions for proposition 2 hold. Given the initial condition

$$\begin{aligned} &1 \leq \Psi(\mathbf{R}(0), \mathbf{R}_d(0)) < 2, \\ &\|\mathbf{e}_\omega(0)\|^2 < \frac{2}{\lambda_{\max}(\mathbf{J})} k_R (2 - \Psi(\mathbf{R}(0), \mathbf{R}_d(0))), \end{aligned} \tag{36}$$

the zero equilibrium of the complete dynamics is exponentially attractive.

Proof: See Appendix A.3.

5. SIMULATION AND RESULTS

We now present the results of numerical simulations to demonstrate the controller's performance. The dynamics of the multirotor with collective pitch-tilting was modeled according to (1) - (4). The physical parameters of the vehicle were set as

$$m = 1\text{kg}, \tag{37}$$

$$\mathbf{J} = \text{diag}(0.0080,\ 0.0039,\ 0.0108)\text{kg}\cdot\text{m}^2. \tag{38}$$

Within the simulation, a desired trajectory was defined, and the vehicle was controlled using the geometric tracking controller to follow the desired trajectory. The parameters for the controller were set to satisfy the conditions in Propositions 1 to 3.

$$k_x = 12,\ k_v = 10,\ k_R = 5,\ k_\omega = 1. \tag{39}$$

Three simulations were conducted, each demonstrating a different capability of the controller. The simulations were all conducted using MATLAB.

Simulation 1: The first simulation demonstrates the proposed controller's ability to follow the desired position trajectory independent of the yaw and pitch. The vehicle was set to move along an upward spiral trajectory while keeping both yaw and pitch constant.

$$\begin{aligned} &\mathbf{x}_d(t) = \left[\cos\left(\frac{\pi}{5}t\right),\ \sin\left(\frac{\pi}{5}t\right),\ t - \frac{1}{2}\right], \\ &\psi_d(t) = 0,\ \theta_d(t) = 0 \end{aligned} \tag{40}$$

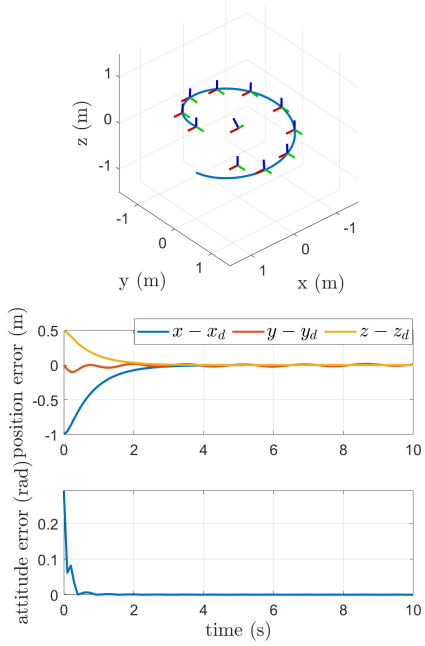

Fig. 4. Result of simulation 1

In this simulation, the initial conditions were set as

$$\begin{aligned} &\mathbf{x}(0) = \mathbf{v}(0) = \boldsymbol{\omega}(0) = [0\ 0\ 0]^T, \\ &\mathbf{R}(0) = \text{Rot}_x\left(\frac{\pi}{4}\right). \end{aligned} \tag{41}$$

The results of Simulation 1 are shown in Fig. 4. The plot on the top displays the vehicle's trajectory, with the blue curve representing the desired trajectory. The vehicle's body frame axes are plotted every second, with the axes colors defined as in Fig. 2. The plot on the bottom shows the trajectory errors over time; the top plot shows the position error, whereas the bottom plot displays the attitude error Ψ. Both the position error and the attitude error are observed to exponentially converge to zero, which is in agreement with Proposition 2, as $\Psi(0) < 1$. This confirms that the vehicle can follow the desired position independent of the yaw and pitch.

Simulation 2: Simulation 2 shows that our controller can control the yaw and pitch independent of the vehicle's position trajectory. For this purpose, the vehicle was set to track the following yaw and pitch angle while it hovers.

$$\begin{aligned} &\mathbf{x}_d(t) = [0\ 0\ 1]^T, \\ &\psi_d(t) = \frac{\pi}{5}t,\ \theta_d(t) = \sin\left(\frac{2\pi}{5}t\right). \end{aligned} \tag{42}$$

The initial condition of the vehicle was set to be stationary, with errors in roll, pitch, and yaw.

$$\begin{aligned} &\mathbf{x}(0) = \mathbf{v}(0) = \boldsymbol{\omega}(0) = [0\ 0\ 0]^T, \\ &\mathbf{R}(0) = \text{Rot}_z\left(\frac{\pi}{2}\right)\text{Rot}_y\left(\frac{\pi}{4}\right)\text{Rot}_x\left(\frac{\pi}{4}\right) \end{aligned} \tag{43}$$

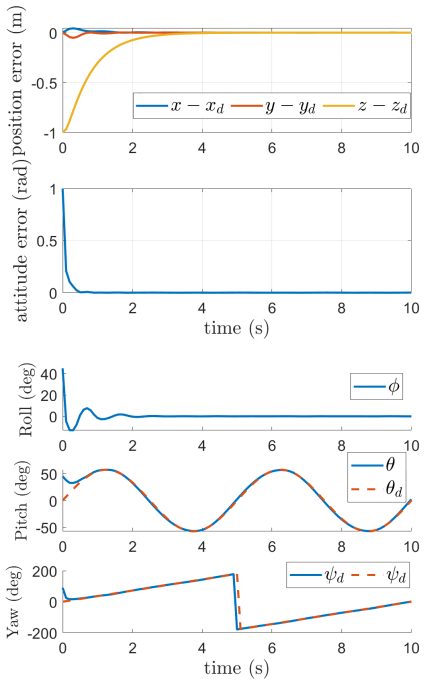

Fig. 5. Result of simulation 2

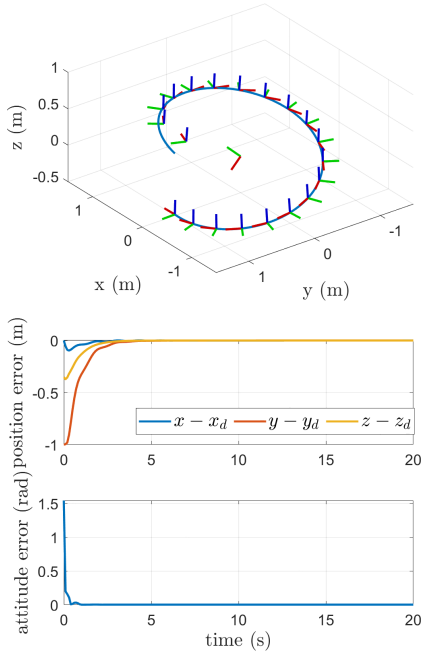

Fig. 6. Result of simulation 3

Fig. 5 presents the results of this simulation. The trajectory plot is omitted since the vehicle was commanded to hover. The plot on the top shows the position and attitude error, whereas the plot on the bottom shows the desired and actual Euler angles. The roll angle has no desired value, as it is not defined in the trajectory. Given that the initial attitude error $\Psi(0) < 1$, the position error and the attitude error both exponentially converge to zero, as predicted by Proposition 2. The ability to maintain zero position and attitude error verifies that the yaw and pitch can be controlled independently of the vehicle's position. Thus, Simulations 1 and 2 demonstrate that the proposed geometric controller can independently track the flat output trajectory as defined in Section 3.

Simulation 3: In this simulation, we demonstrate the overall stability of our controller with large initial attitude errors. The desired position was set as a Lissajous curve, and the desired pitch and yaw were set to point the vehicle roughly in the direction of travel.

$$\begin{aligned} \mathbf{x}_d(t) &= [\sin(at),\ \cos(at),\ 0.5\sin(bt+d)]^T, \\ \psi_d(t) &= -at, \\ \theta_d(t) &= -0.1\cos(bt+d) \end{aligned} \tag{44}$$

For this simulation, the trajectory parameters were set as

$$a = \frac{\pi}{10},\ b = \frac{\pi}{15},\ d = \frac{\pi}{4}. \tag{45}$$

The initial attitude was set to be $1 < \Psi(\mathbf{R}(0), \mathbf{R}_d(0)) < 2$ to demonstrate the stability even with an initial attitude error larger than 90°. The initial condition of the vehicle was set to be the following.

$$\begin{aligned} \mathbf{x}(0) = \mathbf{v}(0) = \boldsymbol{\omega}(0) &= [0\,0\,0]^T, \\ \mathbf{R}(0) &= \mathrm{Rot}_z\left(\frac{\pi}{2}\right)\mathrm{Rot}_y\left(\frac{\pi}{4}\right)\mathrm{Rot}_x\left(\frac{3\pi}{4}\right) \end{aligned} \tag{46}$$

Fig. 6 shows the results of Simulation 3, with the plots organized identically to Fig. 4. Both the position and attitude errors are observed to converge to zero, with the attitude error exhibiting much faster convergence. The attitude error, which has an initial value larger than 1, is shown to decrease exponentially to zero, in agreement with Proposition 2. As the attitude error decreases to below 1 within a finite amount of time, the position error is also able to converge to zero, confirming the exponential attractiveness predicted by Proposition 3.

To demonstrate the superior performance of our controller, we present a comparison with another controller proposed in [11], which is also designed for the multirotor with collective pitch-tilting. This controller is based on PID control on the attitude error, represented by Euler angles.

This controller was tested using the same desired trajectory as shown in (44), but with modified initial conditions: $\mathbf{R}(0) = \mathrm{Rot}_z\left(\frac{\pi}{4}\right)\mathrm{Rot}_y\left(\frac{\pi}{4}\right)\mathrm{Rot}_x\left(\frac{\pi}{4}\right)$. The initial roll error was reduced to avoid the singularity issue when the roll angle is 90°. The initial yaw error was likewise reduced. Without these modifications, the controller exhibits divergence. The gains for the simulated controller, denoted as in [11], are provided in the equation below. The integral

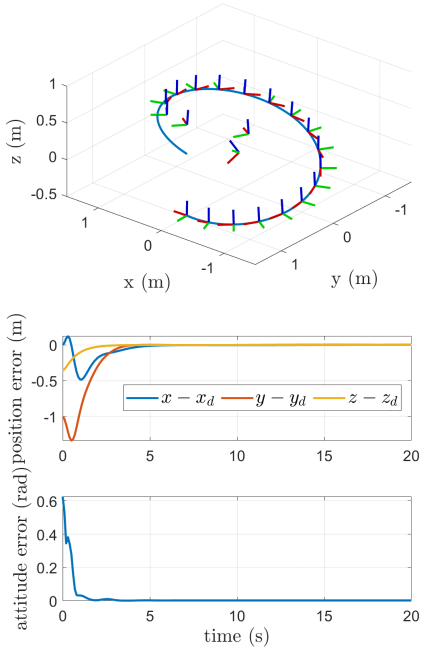

Fig. 7. Result of the reference controller simulation

gains were set to zero to fairly compare with our controller, which does not include an integral error term.

$$\begin{aligned} K_{up} &= 12, \\ K_{ud} &= 10, \\ K_{fp} &= [12\ 12\ 20\ 20\ 8], \\ K_{fd} &= [10\ 10\ 15\ 15\ 2] \end{aligned} \tag{47}$$

The results of this simulation are shown in Fig. 7. Compared to the results from Simulation 3, the reference controller exhibits greater undershoots and slower convergence. These behaviors can be attributed to its weaker stability properties. Specifically, the reference controller is asymptotically stable, whereas our controller demonstrates exponential stability under this simulation's initial conditions. Furthermore, the reference controller's reliance on state transformations complicates the tuning of its parameters.

The reference controller also has a smaller region of stability compared to our controller. Its reliance on inverse matrices makes it vulnerable to singularities, which occur when the determinant of the matrix becomes zero, specifically when the pitch(θ) or roll(ϕ) reach 90°. Consequently, the reference controller can only stabilize the vehicle only within the region $0 \leq \theta, \phi < \frac{\pi}{2}$, whereas our controller remains effective even with a near-inverted initial attitude. This limitation necessitated changing the initial roll angle from $\frac{3\pi}{4}$ to $\frac{\pi}{4}$, as the reference controller cannot recover from such a large initial roll angle. Simulation 3 highlights the versatility of our controller, demonstrating its ability to stabilize the vehicle under conditions where the reference controller fails.

6. CONCLUSION

This study presented a geometric tracking controller for a multirotor with collective pitch-tilting, defined as a multirotor with the capability to generate thrust in the forward direction of the vehicle by tilting the rotors collectively. We showed that the vehicle dynamics is differentially flat, with its center of mass, position, yaw angle, and pitch angle being the flat outputs. A geometric tracking controller was developed based on the rotation matrix representation, thereby circumventing the singularities associated with Euler angles. The vehicle under control was proven to be exponentially stable around the zero error equilibrium with regards to both attitude and position if the attitude error was less than 90°. With an initial attitude error between 90° and 180° the tracking errors were shown to be exponentially attractive. Numerical simulations of the controller confirmed the theoretical performance, demonstrating the controller's capability to recover the vehicle from a roll angle of 135°, a maneuver that a comparative reference controller could not perform.

Future studies should evaluate the performance of the controller in real world environments. This study is based on an ideal vehicle model, with a constant moment of inertia $\mathbf{J}$, unbounded input, and no consideration of unmodeled dynamics. Addressing these limitations and studying their effects will be essential before deploying the controller in practical applications.

APPENDIX A

1. PROOF OF PROPOSITIONS

A.1. Proof of Proposition 1

In terms of attitude, the multirotor with collective pitch-tilting shares the same dynamics and control input as the quadrotor. Consequently, the proof of Proposition 1 as outlined by Lee holds in the same manner [18]. Here, only the Lyapunov function used for the proof is shown, as it is used in a later proof.

$$V_2 = \frac{1}{2}\mathbf{e}_\omega \cdot \mathbf{J}\mathbf{e}_\omega + k_R \Psi(\mathbf{R}, \mathbf{R}_d) + c_2 \mathbf{e}_R \cdot \mathbf{e}_\omega \tag{A.1}$$

The proof shows that $\dot{V}_2 \leq -\beta_2 V_2$ for some $\beta_2 > 0$, proving the exponential stability of the attitude controller.

A.2. Proof of Proposition 2

The proof of Proposition 2 consists of four parts.

a) Attitude Dynamics Error
b) Position and Velocity Error Dynamics
c) Lyapunov Candidate for the Translation Dynamics

d) Lypanunov Function for the Whole System

a) Attitude Error Dynamics: Under the assumptions of Proposition 2, Proposition 1 also holds. From the proof of Proposition 1, $\dot{V}_2|_{c_2=0}(t) < 0$, meaning $\leq V_2|_{c_2=0}(t) \leq V_2|_{c_2=0}(0)$. Combining this with the initial condition given by (33), the following statement holds.

$$k_R \Psi(\mathbf{R}(t), \mathbf{R}_d(t)) \leq V_2|_{c_2=0}(t) \leq V_2|_{c_2=0}(0) < k_R \quad \text{(A.2)}$$

This guarantees the existence of a constant ψ_1 such that

$$\Psi(\mathbf{R}(t), \mathbf{R}_d(t)) \leq \psi_1 < 1 \quad \text{(A.3)}$$

for all t. This means that under the initial conditions specified in Proposition 1, the attitude error remains below 90°.

b) Position and Velocity Error Dynamics: The next step of the proof involves the dynamics of the velocity error $\mathbf{e}_v$. The derivative of $\mathbf{e}_v$ is

$$m\dot{\mathbf{e}}_v = m\ddot{\mathbf{x}} - m\ddot{\mathbf{x}}_d = f_x R\mathbf{e}_1 + f_z R\mathbf{e}_3 - mg\mathbf{e}_3 - m\ddot{\mathbf{x}}_d. \quad \text{(A.4)}$$

Using the definition of $\mathbf{f}_{des}$ given by (21),

$$m\dot{\mathbf{e}}_v = -k_x\mathbf{e}_x - k_v\mathbf{e}_v + \mathbf{a}, \quad \text{(A.5)}$$

where

$$\begin{aligned}\mathbf{a} &= f_x\mathbf{R}\mathbf{e}_1 + f_x\mathbf{R}\mathbf{e}_3 - \mathbf{f}_{des} \\ &= (\mathbf{f}_{des}\cdot\mathbf{R}\mathbf{e}_1)\mathbf{R}\mathbf{e}_1 + (\mathbf{f}_{des}\cdot\mathbf{R}\mathbf{e}_3)\mathbf{R}\mathbf{e}_3 - \mathbf{f}_{des} \\ &= -(\mathbf{f}_{des}\cdot\mathbf{R}\mathbf{e}_2)\mathbf{R}\mathbf{e}_2.\end{aligned} \quad \text{(A.6)}$$

The next part requires the following lemma.

Lemma 1: For a given rotation matrix $\mathbf{R}, \mathbf{R}_d \in \mathrm{SO}(3)$, the following equation holds for any unit vector $\mathbf{x}$.

$$1 - \Psi(\mathbf{R}, \mathbf{R}_d) \leq \mathbf{x}^T\mathbf{R}_d^T\mathbf{R}\mathbf{x} \leq 1 \quad \text{(A.7)}$$

Proof: The rotation matrix $\mathbf{R}_d^T\mathbf{R}$ represents a rotation from the desired orientation to the actual body orientation. In 3D space, any rotation can be expressed as a rotation of angle θ around a given unit vector $\mathbf{u}$ which serves as the rotation axis. Using the Rodrigues' rotation formula, it can be shown that $1-\Psi = \cos(\theta)$. Finally, the unit vector $\mathbf{x}$ is decomposed into components parallel and perpendicular to the rotation axis, such that $\mathbf{x} = x_u\mathbf{u} + x_v\mathbf{v}$. By applying these concepts to (A.7), we obtain

$$\begin{aligned}&\mathbf{x}^T\mathbf{R}_d^T\mathbf{R}\mathbf{x} = \mathbf{x}\cdot(\mathbf{R}_d^T\mathbf{R}\mathbf{x}) \\ &= (x_u\mathbf{u} + x_v\mathbf{v})\cdot(x_u\mathbf{u} + x_v\mathbf{R}_d^T\mathbf{R}\mathbf{v}) = x_u^2 + x_v^2\cos(\theta).\end{aligned} \quad \text{(A.8)}$$

Since $x_u^2 + x_v^2 = 1$, $x_u^2 + x_v^2\cos(\theta) \leq 1$, this proves lemma 1.

c) Lyapunov Candidate for the Translation Dynamics: Given a positive c_1, the Lyapunov candidate for the translation dynamics is defined as

$$V_1 = \frac{1}{2}k_x\|\mathbf{e}_x\|^2 + \frac{1}{2}m\|\mathbf{e}_v\|^2 + c_1\mathbf{e}_x\cdot\mathbf{e}_v. \quad \text{(A.9)}$$

The derivative of V_1 under the error dynamics of the multirotor with collective pitch-tilting is

$$\begin{aligned}\dot{V}_1 = &-(k_v - c_1)\|\mathbf{e}_v\|^2 - \frac{c_1k_x}{m}\|\mathbf{e}_x\|^2 \\ &- \frac{c_1k_v}{m}\mathbf{e}_x\cdot\mathbf{e}_v + \mathbf{a}\cdot\left\{\frac{c_1}{m}\mathbf{e}_x + \mathbf{e}_v\right\}.\end{aligned} \quad \text{(A.10)}$$

A bound for $\mathbf{a}$ will now be specified. First, define a unit vector as $\mathbf{u}_{des} = \frac{\mathbf{f}_{des}}{\|\mathbf{f}_{des}\|}$. Then the bound can initially be set as

$$\|\mathbf{a}\| = \|\mathbf{f}_{des}\cdot\mathbf{R}\mathbf{e}_2\| \leq \|\mathbf{f}_{des}\|\|\mathbf{u}_{des}\cdot\mathbf{R}\mathbf{e}_2\| \quad \text{(A.11)}$$

The desired attitude was set such that the thrust in the $\mathbf{b}_1, \mathbf{b}_3$ direction would be able to generate the desired force $\mathbf{f}_{des}$ in its entirety. Consequently, $\mathbf{f}_{des}$ lies within the plane defined by $\mathbf{R}_d\mathbf{e}_1, \mathbf{R}_d\mathbf{e}_3$ and therefore $\mathbf{f}_{des}\cdot\mathbf{R}_d\mathbf{e}_2 = 0$. Equivalently, $\mathbf{u}_{des}\cdot\mathbf{R}_d\mathbf{e}_2 = 0$.

Let's now split $\mathbf{R}\mathbf{e}_2$ into the components parallel and perpendicular to $\mathbf{R}_d\mathbf{e}_2$, such that $\mathbf{R}\mathbf{e}_2 = \phi_2\mathbf{R}_d\mathbf{e}_2 + \phi_{13}\mathbf{u}_{13}$. Here $\mathbf{u}_{13}$ is a unit vector perpendicular to $\mathbf{R}_d\mathbf{e}_2$, meaning $\mathbf{u}_{13}\cdot\mathbf{R}_d\mathbf{e}_2 = 0$. From lemma 1, the inequality

$$1 - \Psi \leq \mathbf{e}_2^T\mathbf{R}_d^T\mathbf{R}\mathbf{e}_2 = \phi_2 \leq 1 \quad \text{(A.12)}$$

holds. Consequently, the inequality

$$0 \leq \phi_{13} \leq \sqrt{\Psi(2-\Psi)} \quad \text{(A.13)}$$

also holds. Applying this to (A.11) yields

$$\|\mathbf{a}\| \leq \|\mathbf{f}_{des}\|\|\phi_{13}\mathbf{u}_{des}\cdot\mathbf{u}_{13}\| \leq \sqrt{\Psi(2-\Psi)} \quad \text{(A.14)}$$

since $\mathbf{u}_{des}\cdot\mathbf{u}_{13} \leq 1$.

From (A.3), $\sqrt{\Psi(2-\Psi)} \leq \sqrt{\psi_1(2-\psi_1)} < 1$. In addition, the inequality $\|\mathbf{f}_{des}\| \leq (k_x\|\mathbf{e}_x\| + \|k_v\|\mathbf{e}_v\| + B)$ holds. Using both inequalities, the bound for $\mathbf{a}$ can be expressed as

$$\|\mathbf{a}\| \leq \|\mathbf{f}_{des}\|\|\mathbf{u}_{des}\cdot\mathbf{R}\mathbf{e}_2\| \leq (k_x\|\mathbf{e}_x + \|k_v\|\mathbf{e}_v\| + B)\alpha. \quad \text{(A.15)}$$

The dynamics of V_1 can now be bounded using the bound of $\mathbf{a}$.

$$\begin{aligned}\dot{V}_1 \leq &-(k_v(1-\alpha) - c_1)\|\mathbf{e}_v\|^2 - \frac{c_1k_x}{m}(1-\alpha)\|\mathbf{e}_x\|^2 \\ &+ \frac{c_1k_v}{m}(1+\alpha)\|\mathbf{e}_x\|\|\mathbf{e}_v\| \\ &+ \|\mathbf{e}_R\|\left\{k_x\|\mathbf{e}_x\|\|\mathbf{e}_v\| + \frac{c_1}{m}B\|\mathbf{e}_x\| + B\|\mathbf{e}_v\|\right\}\end{aligned} \quad \text{(A.16)}$$

The above inequality would be a quadratic inequality if not for the term $k_x\|\mathbf{e}_x\|\|\mathbf{e}_v\|\|\mathbf{e}_R\|$. This term is bounded using the assumption that $\|\mathbf{e}_x\| < e_{x_{\max}}$.

d) Lypanunov Function for the Whole System: The Lyapunov function for the whole system is defined as $V = V_1 + V_2$.

$$V = \frac{1}{2}k_x\|\mathbf{e}_x\|^2 + \frac{1}{2}m\|\mathbf{e}_v\|^2 + c_1\mathbf{e}_x\cdot\mathbf{e}_v + \frac{1}{2}\mathbf{e}_\omega\cdot\mathbf{J}\mathbf{e}_\omega + k_R\Psi(\mathbf{R},\mathbf{R}_d) + c_2\mathbf{e}_R\cdot\mathbf{e}_\omega \quad \text{(A.17)}$$

Using the results from the proof of Proposition 1, a bound for the Lyapunov function V can be set as

$$\mathbf{z}_1^T\mathbf{M}_{11}\mathbf{z}_1 + \mathbf{z}_2^T\mathbf{M}_{21}\mathbf{z}_2 \le V \le \mathbf{z}_1^T\mathbf{M}_{12}\mathbf{z}_1 + \mathbf{z}_2^T\mathbf{M}_{22}\mathbf{z}_2 \quad \text{(A.18)}$$

where $\mathbf{z}_1 = [\|\mathbf{e}_x\|,\ \|\mathbf{e}_v\|]^T$, $\mathbf{z}_2 = [\|\mathbf{e}_R\|,\ \|\mathbf{e}_\omega\|]^T$ and the matrices $\mathbf{M}_{11},\mathbf{M}_{12},\mathbf{M}_{21},\mathbf{M}_{22}$ are defined as

$$\mathbf{M}_{11} = \frac{1}{2}\begin{bmatrix} k_x & -c_1 \\ -c_1 & m \end{bmatrix},\ \mathbf{M}_{12} = \frac{1}{2}\begin{bmatrix} k_x & c_1 \\ c_1 & m \end{bmatrix},$$
$$\mathbf{M}_{21} = \frac{1}{2}\begin{bmatrix} k_R & -c_2 \\ -c_2 & \lambda_{\min}(\mathbf{J}) \end{bmatrix},\ \mathbf{M}_{22} = \frac{1}{2}\begin{bmatrix} \frac{2k_R}{2-\psi_1} & c_2 \\ c_2 & \lambda_{\max}(\mathbf{J}) \end{bmatrix}. \quad \text{(A.19)}$$

Using (A.16) and the results from the proof of Proposition 1, the derivative of V is

$$\dot{V} = -\mathbf{z}_1^T\mathbf{W}_1\mathbf{z}_1 + \mathbf{z}_1^T\mathbf{W}_{12}\mathbf{z}_2 - \mathbf{z}_2^T\mathbf{W}_2\mathbf{z}_2 \quad \text{(A.20)}$$

where $\mathbf{W}_1,\mathbf{W}_{12},\mathbf{W}_2$ are the matrices defined in (29).

Under the initial conditions given by 30, 31, 32, the matrices $\mathbf{M}_{11},\mathbf{M}_{12},\mathbf{M}_{21},\mathbf{M}_{22},\mathbf{W}_1,\mathbf{W}_2$ are positive definite. Consequently, V is positive definite, and the derivative $\dot{V}$ is negative definite. Therefore, the zero equilibrium of the tracking errors is exponentially stable.

A.3. Proof of Proposition 3

Proposition 1 states that given the initial conditions of (36), the attitude errors $\mathbf{e}_R,\mathbf{e}_\Omega$ exponentially converge to zero. Therefore, there exists a time t^*, such that when $t > t^*$, $\Psi(\mathbf{R}(t),\mathbf{R}_d(t)) < 1$, where Proposition 2 now holds. Thus, by showing $\mathbf{e}_x,\mathbf{e}_v$ is bounded within $0 < t < t^*$, all of the errors are guaranteed to be bounded. Since all of the errors exponentially decrease at $t > t^*$, the system is then exponentially attractive.

The proof of the boundness of $\mathbf{z}_1 = [\|\mathbf{e}_x\|,\ \|\mathbf{e}_v\|]^T$ is as follows. Consider the translational error dynamics

$$m\dot{\mathbf{e}}_v = f_x R\mathbf{e}_1 + f_z R\mathbf{e}_3 - mg\mathbf{e}_3 - m\ddot{\mathbf{x}}_d. \quad \text{(A.21)}$$

Define a positive definite Lyapunov function V_3 as

$$V_3 = \frac{1}{2}\|\mathbf{e}_x\|^2 + \frac{1}{2}m\|\mathbf{e}_v\|^2. \quad \text{(A.22)}$$

Naturally, the inequalities $\|\mathbf{e}_x\| \le \sqrt{2V_3}$, $\|\mathbf{e}_v\| \le \sqrt{\frac{2}{m}V_3}$ hold. The derivative of V_3 is

$$\dot{V}_3 = \mathbf{e}_x\cdot\mathbf{e}_v + \mathbf{e}_v\cdot(f_x\mathbf{R}\mathbf{e}_1 + f_z\mathbf{R}\mathbf{e}_3 - mg\mathbf{e}_3 - m\ddot{\mathbf{x}}_d). \quad \text{(A.23)}$$

Equations (20), (A.5), and (A.15) yield the following inequality.

$$\begin{aligned}\dot{V}_3 &\le \|\mathbf{e}_x\|\|\mathbf{e}_v\| + \|\mathbf{e}_v\|B + \|\mathbf{e}_v\|(k_x\|\mathbf{e}_x\| + k_v\|\mathbf{e}_v\| + B) \\ &= k_v\|\mathbf{e}_v\|^2 + \|\mathbf{e}_v\|(2B + (k_x+1)\|\mathbf{e}_x\|)) \\ &\le d_1V_3 + d_2\sqrt{V_3}\end{aligned} \quad \text{(A.24)}$$

where $d_1 = \frac{2k_V}{m} + \frac{2(k_x+1)}{\sqrt{m}}$, $d_2 = 2B\sqrt{\frac{2}{m}}$.

Now assume there is a time interval $[t_0,t_1] \subset [0,t^*]$ where $V_3(t) \ge 1$. Here, $\sqrt{V_3} \le V_3$, which yields

$$\begin{aligned}\dot{V}_3 &\le (d_1+d_2)V_3 \\ V_3 &\le V_3(t_0)e^{(d_1+d_2)(t-t_0)}.\end{aligned} \quad \text{(A.25)}$$

This shows that within $0 < t < t^*$, V_3 remains bounded. Consequently, $\mathbf{z}_1$ is also bounded, concluding the proof.

CONFLICT OF INTEREST

Dongjun Lee is a Senior Editor of the International Journal of Control, Automation, and Systems. Senior Editor status has no bearing on editorial consideration. The authors declare that there is no competing financial interest or personal relationship that could have appeared to influence the work reported in this paper.

REFERENCES

[1] S. Tang and V. Kumar, "Autonomous flight," *Annual Review of Control, Robotics, and Autonomous Systems*, vol. 1, pp. 29–52, 2018.

[2] M. W. Mueller, S. J. Lee, and R. D'Andrea, "Design and control of drones," *Annual Review of Control, Robotics, and Autonomous Systems*, vol. 5, pp. 161–177, 2022.

[3] M. Hamandi, F. Usai, Q. Sablé, N. Staub, M. Tognon, and A. Franchi, "Design of multirotor aerial vehicles: A taxonomy based on input allocation," *The International Journal of Robotics Research*, vol. 40, no. 8-9, pp. 1015–1044, 2021.

[4] M. Allenspach, K. Bodie, M. Brunner, L. Rinsoz, Z. Taylor, M. Kamel, R. Siegwart, and J. Nieto, "Design and optimal control of a tiltrotor micro-aerial vehicle for efficient omnidirectional flight," *The International Journal of Robotics Research*, vol. 39, no. 10-11, pp. 1305–1325, 2020.

[5] S. Park, J. Lee, J. Ahn, M. Kim, J. Her, G.-H. Yang, and D. Lee, "Odar: Aerial manipulation platform enabling omnidirectional wrench generation," *IEEE/ASME Transactions on mechatronics*, vol. 23, no. 4, pp. 1907–1918, 2018.

[6] M. Ryll, G. Muscio, F. Pierri, E. Cataldi, G. Antonelli, F. Caccavale, and A. Franchi, "6d physical interaction with a fully actuated aerial robot," in *2017 IEEE International Conference on Robotics and Automation (ICRA)*, pp. 5190–5195, IEEE, 2017.

[7] S. J. Lee, D. Lee, J. Kim, D. Kim, I. Jang, and H. J. Kim, "Fully actuated autonomous flight of thruster-tilting multirotor," *IEEE/ASME Transactions on Mechatronics*, vol. 26, no. 2, pp. 765–776, 2020.

[8] K. Kawasaki, Y. Motegi, M. Zhao, K. Okada, and M. Inaba, "Dual connected bi-copter with new wall trace locomotion feasibility that can fly at arbitrary tilt angle," in *2015 IEEE/RSJ International Conference on Intelligent Robots and Systems (IROS)*, pp. 524–531, IEEE, 2015.

[9] T. Fukuda, A. Sakaguchi, T. Takimoto, and T. Ushio, "Modeling and stabilization of the novel quadrotor with tilting propeller," in *Proc. Symposium on Nonlinear Theory and Its Applications*, pp. 173–176, 2016.

[10] H. Paul, R. R. Martinez, B. Sumetheeprasit, and K. Shimonomura, "A tiltable airframe multirotor uav designed for omnidirectional aerial manipulation," in *2023 IEEE/ASME International Conference on Advanced Intelligent Mechatronics (AIM)*, pp. 460–465, IEEE, 2023.

[11] D. Lee, S. Hwang, C. Kim, S. J. Lee, and H. J. Kim, "Minimally actuated tiltrotor for perching and normal force exertion," in *2023 IEEE/RSJ International Conference on Intelligent Robots and Systems (IROS)*, pp. 5027–5033, IEEE, 2023.

[12] T. Lee, M. Leok, and N. H. McClamroch, "Geometric tracking control of a quadrotor uav on se (3)," in *49th IEEE conference on decision and control (CDC)*, pp. 5420–5425, IEEE, 2010.

[13] D. Invernizzi and M. Lovera, "Geometric tracking control of a quadcopter tiltrotor uav," *IFAC-PapersOnLine*, vol. 50, no. 1, pp. 11565–11570, 2017.

[14] R. Mahony, V. Kumar, and P. Corke, "Multirotor aerial vehicles: Modeling, estimation, and control of quadrotor," *IEEE robotics & automation magazine*, vol. 19, no. 3, pp. 20–32, 2012.

[15] D. Mellinger and V. Kumar, "Minimum snap trajectory generation and control for quadrotors," in *2011 IEEE international conference on robotics and automation*, pp. 2520–2525, IEEE, 2011.

[16] F. Bullo and A. D. Lewis, *Geometric control of mechanical systems: modeling, analysis, and design for simple mechanical control systems*, vol. 49. Springer, 2019.

[17] Z. Qu, *Robust control of nonlinear uncertain systems*. John Wiley & Sons, Inc., 1998.

[18] T. Lee, M. Leok, and N. H. McClamroch, "Control of complex maneuvers for a quadrotor uav using geometric methods on se (3)," *arXiv preprint arXiv:1003.2005*, 2010.

Jongann Lee is an undergraduate student at Seoul National Univesity, Seoul, Korea. He is working toward a B.S. degree in aerospace engineering. His current research interests include mobile robotics, control engineering, reinforcement learning, and safety in control.

Taekyun Kim received his B.S. degree in mechanical engineering from Seoul National University, Seoul, Korea in 2020, where he is currently working toward a Ph.D. degree in mechanical engineering. His research interests include state estimation of mobile robots, aerial manipulation system and cooperative manipulation.

Dongjun Lee received his B.S. degree in mechanical engineering and an M.S. degree in automation and design from the Korea Advanced Institute of Science and Technology, Daejeon, Korea, and a Ph.D. degree in mechanical engineering from the University of Minnesota at Twin Cities, Minneapolis, MN, USA, 2004. He is currently a Professor with the Department of Mechanical Engineering, Seoul National University, Seoul, Korea. His research interests include the dynamics and control of robotic and mechatronic systems with emphasis on aerial/mobile robots, teleoperation/haptics, physics simulation, multirobot systems, and industrial control applications.